Author response to referee comments

We would like to thank both reviewers for their thorough and constructive comments on our manuscript and for recognising the positive contribution the paper can make to understanding of the nature of biomass burning emissions in Africa. We believe that implementation of the suggestions made by the referees has greatly improved the presentation of the revised paper. Referee comments are addressed in turn below. The original comments are coloured red and author comments coloured black.

Referee 1:

Specific Comments:

This paper uses OLS regression, which is inappropriate for calculating trace gas ratios. While OLS is scale invariant, ratios taken from the slope of this regression cannot be inverted. Since all OLS regressions presented in this paper use observed data, a weighted regression (such as the York regression; please see York et al. 2004, Cantrell 2008, and Wu and Yu 2018, references below) using instrument precision as the variable weights will provide a robust trace gas ratio that is both scale invariant and slope invertible. Please do not use unweighted orthogonal distance regression (ODR) in place of OLS for trace gas ratios, as ODR is sensitive to the scales of the axes.

We agree that the use of OLS regression may not be optimal for the determination of trace gas emission ratios as was done in the original manuscript. York et al., 2004, regressions have now been implemented in place of the OLS fits in Figure 11 following the reviewer's suggestion. Very slight changes in final emission factors and their respective uncertainties are now seen compared with the original OLS approach.

The emission factors calculated in this paper use a single value for the mass fraction of the dry fuel. With the context that the primary fuel is changing from C3 to C4 plants between MOYA-I and MOYA-II, is this single mass fraction appropriate for both regions?

This potential difference was indeed considered in previous iterations of the manuscript, but estimating fuel carbon fractions for each study area in lieu of a more detailed knowledge of the fuels was not possible. We were unable to find literature carbon fractions that were more representative of the study areas/fuel mixtures encountered during this work. Previous aircraft biomass burning studies such as Yokelson et al. 2009 have also used a single carbon fraction value for fires originating from different fuels, but have included a ±10% uncertainty range to account for potential error due to this fuel uncertainty. To be consistent with previous studies, we have now implemented a ±10% uncertainty into our carbon fraction to account for differences in fuel carbon content between the study areas. This uncertainty is propagated through to the final emission factors presented in the revised paper. The difference between methane emissions (between different areas) remains significant (outside of error) after this change.

1

35   I have some question about whether figure 6 is currently adding significantly to the discussion. In its current formulation this figure is only applicable to the MOYA-II flights, and the B panel is repeating information that it shown with better context in Figure 1. If a similar ground cover map for Senegal was available keeping figure 6 as a ground cover discussion would be useful, but in its current form figure 6 could be moved to the supplementary material without impacting the discussion.

40   We acknowledge that Figure 6 is a relatively weak figure in its original format and does not add much to the discussion. The MODIS fire map of Uganda has now been replaced with a land cover classification map of Senegal, and references and discussion have been added for both land cover classifications.

   For figures 7 and 8, the plots where clearly motivated in the text; I would like to see this analysis applied to the other trace gas
45   species. While the primary motivation of these missions was to quantify methane emissions, extending this analysis to CO, CO2, and the additional MOYA-II species either in these plots or as supplemental material would be a welcome addition to the paper.

   This is an excellent idea. We have added plots of CO_2 and CO emission factor versus modified combustion efficiency to the
50   updated manuscript. A N_2O emission factor vs modified combustion efficiency plot is also included in the SI, where no linear relationship was observed.

   The Far Field Sampling section feels moderately unorganized compared to the rest of section 4. Currently the paper discusses the two flights separately, with 6 total figures; changing the structure to discussing both flights together by type of analysis
55   (back trajectories, vertical distributions, and trace gas ratios) would allow the authors to combine the plots into three figures and compare and contrast the two flights more effectively.

   We agree. This section did not flow well in its original form, and feels repetitive with separation of the same figure types into individual flights. The back-trajectories, vertical box-whisker plots and trace gas ratios have now been combined from six
60   figures into three separate figures, with each figure encompassing both flights. The discussion text has also been reorganised to discuss by analysis type, rather than by flight.

Technical Corrections and Small Issues:

   There are some minor structural issues the methods sections. Section 2 and 3 would work better as a combined methods section,
65   and I recommend splitting both the CIMS instrument and the WAS measurements into their own individual subsections.

2

We agree. This has now been changed. The two sections have been combined and instrumental methods are now divided into the subsections 'CH$_4$, CO$_2$, CO and N$_2$O Instrumentation', 'HCN and HNCO Instrumentation (Chemical Ionisation Mass Spectrometer)' and 'Whole Air Sampling and Methane Isotopic Analysis'.

70

Was the data used in this paper time synced? This is important for capturing trace gas ratios from regression methodology and should be included in the methods.

All aircraft instrumentation is synced to a time server on-board the aircraft, and WAS capture start and end times are recorded

75 using the time from this time server. This information has now been added to the revised methods section.

Since the identification of the plumes was done with statistics above the background, how was the "width" of the plume assigned? Is the plume only valid when your tracer species is at or above the threshold, or is the plume assigned with some buffer time on either side?

80

Despite using a statistical concentration threshold to select plumes, identifying a 'catch all' single method to assign plume width and background areas for all plumes proved difficult due to the individual systematic differences between plumes and area above the threshold. Near-field plume start and end time, as well as background regions, were assigned manually using the data. The statistical threshold was only used to automate and identify the plumes for further analytical treatment. This has

85 now been clarified in the 'Calculation of Emission Ratios and Emission Factors' subsection.

Figure 2 is out of order – it's cited after Figures 3 and 4.

Thank you. This has been corrected.

90

In Figure 4 was the linear relationship applied to all measurements in the C004 and C005 flights, or did it leave off the high inverse CH4 data? If some data was left off, what was the threshold for that decision?

Upon further examination of the WAS times, some WAS points have now been discarded from the analysis due to samples

95 being taken on the ground or too close to Dakar (potentially influenced by urban emissions) on the profile ascent out of the airport to the study area. The linear fit is now applied to all remaining points of the C005 WAS samples. We have decided to remove the singular C004 point from the fit, as a single point is not useful in constraining a linear relationship. The updated Figure 4 is now included in the manuscript.

100

We agree that this would be much clearer if illustrated in a figure. The strong linear relationship between EF and MCE is shown
105 clearly in figure 7, which is coloured by each flight. We think a separate EF vs MCE graph for the mean EFs and MCEs for C132-C134 would essentially be a simplified version of figure 7, so fig. 7 has now been referenced in the statement highlighted by the reviewer.

110

We agree. These have been added.

115 This is a good idea. These have been added to the supplementary information.

120

The back-trajectories are simulated for 60 s intervals during times when biomass burning emissions were observed and sampled (from grey shaded areas in Fig. S5 and S6 in supplementary). The box-whisker plots use 400 m altitude bins. This has now been clarified in the text and captions.

125

130

4

Referee 2:

While there are no obvious spectroscopic interferences of other species with the N_2O spectral absorption feature, the nature of the N_2O instrument issues were perhaps inadequately described in the original manuscript. The Aerodyne QCLAS instrument exhibits a significant known cabin pressure dependency, in which significant changes in altitude, and hence cabin pressure, change the refractive index in the open path section of the laser beam. This can lead to static optical fringes moving across the spectral baseline of the instrument, introducing both long-term drift and short-term artefacts into the N_2O mole fraction data. Also, sharp changes in aircraft roll angle in tight turns can also introduce short-term artefacts as forces acting on optical components cause slight changes in alignment. A further issue encountered solely during the MOYA-II campaign was occasional loss of optical bench temperature control due to the high temperatures experienced within the aircraft during some flights.

Despite these known issues, the N_2O plumes from which EF could be calculated were sampled at constant altitude with wings-level at constant optical bench temperature. So the instrument issues detailed above are expected to have no systematic effect on data quality. More information on these issues has now been added to the text.

We apologise for the lack of clarity in the text here. Background determinations were completed by overflowing N_2 gas just above the moveable critical orifice prior to the IMR, and humidity corrections were applied during post processing of the data, as described in the manuscript. Humidity dependency was determined by varying the IMR humidity while delivering a constant mixing ratio HCN in into the instrument over a range of atmospherically relevant concentrations, which is common practice.

More details have now been added to the text to explain the CIMS design. However, we believe it is not useful to include a diagram due to its simplicity and similarity to the setup of Lee et al. (2018), which is referenced and has a figure included in that study. This is now referenced in the text.

We apologise for the lack of clarity in the text here. The WAS canisters were subsequently analysed for mean $\delta^{13}C$ methane isotope ratio (GC-MS) and mean methane mole fraction (Picarro 1303 Cavity Ringdown IR spectrometer) in the lab. The inverse CH_4 mole fraction used in the Keeling plots is from the lab analysis of the WAS canisters, not from the in situ methane measurements aboard the aircraft. Each point in the Keeling plots is the mean $\delta^{13}C$-CH_4 and mean $1/[CH_4]$ from one canister. Lab and in situ mean CH_4 mole fraction during each WAS sampling period were compared and found to agree within uncertainty (not shown). The use of lab CH_4 instead of in situ CH_4 for Keeling plots has been made clearer in the text.

5

180   Thank you for this suggestion. We agree. This has now been clarified in the revised text. The intercepts from Chanton et al. (2000) are now included; an intercept range of -17 ‰ to -26 ‰ for African grassland burning is shown as a shaded area and an intercept of -30 ‰ for African forest burning is shown as a red dashed line. These simulated fits originate from the start point of the C005 fit.

185   Line 416: The authors suggest that in Uganda the Keeling plot analysis could not be used. Could the authors show a Figure of this in the SI in comparison to Senegal?

        This is a useful idea – thank you. This has been added to the SI.

190   Line 421: I wouldn't consider this a forest rather than a combined forest & grassland area based on this one picture (the quality of the picture is not great). This is also mentioned by the authors later in the text. Please rephrase and consistently mention throughout the manuscript.

195   Agreed. This has been corrected and the suspected mixed nature of the fuel has now been made consistent throughout the manuscript

        Line 419-440: Even if the emissions are a mixture of forest and grassland I don't understand why this wouldn't be consistent for both the isotopic analysis and the EFs. The
200   influence of grassland burning is reflected both in the MCEs and EFs but not the isotopic ratios. What is the isotopic intercept difference of C3 forest litter and C4 tropical grasses and maize? Is the difference dramatic? I think the discussion in this section could be improved by mentioning all the parameters that can affect both the isotopic ratio and EF calculations and then conclude which one is expected to play a dominant
205   role in the observed differences. Also, could these differences be related to different parts of the plume being sampled from the different inlets (CH4 vs Canisters) at different parts of the plain? How far away were the two instrument inlets? If the plumes are not dense could this become an issue?

        This section has been revised to highlight the parameters that affect isotopic ratio and methane EF more clearly. We do not
210   believe differences in plume sampling between in situ CH_4 and WAS CH_4 are the cause for this, however. The plumes encountered during C004 and C005 involved sharp enhancements that in most cases lasted for <20 s. The WAS fill times during these flights were approximately 20 s and captured the majority of the plume in all in-plume WAS samples.

        Line 575: Visual observations don't strongly support this.
215
        We agree. This sentence has been removed.

        Calculation of the slope to CO based on a linear fit is how the authors determine the ERs for the far-flights. It will improve comparisons if the authors apply this approach
220   for the other flights and determine whether they observe any substantial differences compared to equation 1.

        We agree that this would provide important intercomparison and validation for each ER determination method. As an extension of the referee's suggestion, both the linear regression method and the peak integration method have been applied to all flights
225   to give a comprehensive comparison of the two methods. The two methods show very good agreement, with final CH_4 and CO_2

EFs agreeing comfortably within uncertainty for all flights. The far-field flight EF uncertainties calculated using the integration method are significantly larger than other uncertainty ranges due to the high variability of the background mole fraction and relatively low enhancement in the plume compared to those seen in the near-field flights. This analysis is now shown in the revised SI.

230

For final EF reporting, the integration method is still used for near-field flights as this gives ER and EF data for each individual plume, allowing the EF vs MCE analysis to be carried out and reported. Linear regression is still used for far-field ER calculation as the EF uncertainty is minimised.

235 Figure 3: I would recommend restructuring the Fig. in order to make it more instructive. Some suggestions below: Exclude (a) and keep only (b) this way you have a longer timeseries for the reader to look at. Split x-axis to 7 axes that are plotted against the same y-axis. Each x-axis will show an individual plume crossing (in total 7 plumes, 7 x-axes) zoomed in to the respective plume and their backgrounds. Please do the same
240 for Fig. 5 and all the other flights in the SI.

We agree. Figures 3, 5 and those in the SI have now been updated to include split X-axes for each plume, with the plume area zoomed in.

245 Figure 6: It would be informative if the flight tracks are shown in one of the two maps. This graph could also be moved to the SI.

Figure 6 has now been revised to include a land cover classification map for Senegal as well as Uganda (see response to Reviewer #1 also). However, we feel that adding flight tracks to the land cover maps may obscure the land cover classifications,
250 so these remain separate in the revised mauscript.

Figure 7: Would the ratio of HCN / HNCO change depending on the particle humidity and therefore the more efficient uptake to the particles of HNCO? I guess it will not be significant compared to the emission differences but maybe an interesting topic to discuss here.

This is an interesting idea for further investigation and discussion, but this is beyond the scope of the work presented here.

255 Figure 10: Make the extreme markers smaller and grey.

This has now been changed.

Line 259: Maybe delete FIGAERO-CIMS instrument analysis software and just include the ARI Tofware version 3.1.0. Readers may be confused when reading FIGAERO and expect particle-phase measurements

260 We agree with this. This has been changed.

Line 297: delete "an".

Changed. Thank you.

7

Line 301-302: How do you know if the flights display no significant plume ageing? Please specify based on the airborne measurements.

Plume ageing is inferred based on airmass history from HYSPLIT back trajectories from in-plume data for far-field flights as discussed in the text. All near-field flights sampled biomass burning emissions essentially at the source (directly above and
confirmed visually), so no plume ageing was assumed. This has now been clarified in the text.

Line 302: delete "confidently".

Removed.
Line 424: Change "Mean" to "mean".

Changed.
Line 428: Change "It" to "it".

Changed.

Line 437: Delete ".".
Removed.

Line 457: There is inconsistent use of brackets here and at other parts of the manuscript.
Brackets have been made consistent throughout the manuscript.

Line 459: Delete ".".

Removed.

Line 460: Change "," to ".".

Changed.

300

Airborne measurements of fire Emission Factors for African biomass burning sampled during the MOYA Campaign

305 Patrick A. Barker.[1], Grant Allen.[1], Martin Gallagher.[1], Joseph R. Pitt.[2], Rebecca E. Fisher.[3], Thomas Bannan.[1], Euan G. Nisbet.[3], Stéphane J. -B. Bauguitte.[4], Dominika Pasternak.[5], Samuel Cliff.[5], Marina B. Schimpf.[6], Archit Mehra.[1], Keith N. Bower.[1], James D. Lee.[5], Hugh Coe.[1], Carl J. Percival.[7]

[1]School of Earth and Environmental Sciences, University of Manchester, Manchester, M13 9PL, UK.

310 [2]School of Marine and Atmospheric Sciences, 145 Endeavour Hall, Stony Brook University, Stony Brook, NY 11794-5000, USA.

[3]Department of Earth Sciences, Royal Holloway, University of London, Egham, Surrey, TW20 0EX, UK.

[4]FAAM Airborne Laboratory, National Centre for Atmospheric Sciences, Building 146, College Road, Cranfield, MK43 0AL, UK.

315 [5]Wolfson Atmospheric Chemistry Laboratories, Department of Chemistry, University of York, Heslington, York YO10 5DD, UK.

[6]German Aerospace Center (DLR), Flight Experiments, Instrumentation and Data Science, Muenchener Strasse 20, 82234 Wessling, Germany.

[7]Jet Propulsion Laboratory, California Institute of Technology, 4800 Oak Grove Drive, M/S 183-901, Pasadena, California 320 91109, USA.

Correspondence to: Patrick A. Barker (patrick.barker@manchester.ac.uk)

Abstract. Airborne sampling of methane (CH_4), carbon dioxide (CO_2), carbon monoxide (CO), and nitrous oxide (N_2O) mole fractions was conducted during field campaigns targeting fires over Senegal in February and March 2017, and Uganda in 325 January 2019. The majority of fire plumes sampled were close to, or directly over burning vegetation, with the exception of two longer-range flights over the West African Atlantic seaboard, (100 – 300 km from source) where the continental outflow

9

of biomass burning emissions from a wider area of West Africa was sampled. Fire Emission Factors (EFs) and modified combustion efficiencies (MCEs) were estimated from the enhancements in measured mole fractions. For the Senegalese fires, mean EFs and corresponding uncertainties in units of g per kg of dry fuel were 1.8 ± 0.19 for CH_4, 1633 ± 171.4 for CO_2 and 67 ± 7.4 for CO, with a mean MCE of 0.94 ± 0.005. For the Ugandan fires, mean EFs were 3.1 ± 0.35 for CH_4, 1610 ± 169.7 for CO_2 and 78 ± 8.9 for CO, with a mean modified combustion efficiency of 0.93 ± 0.004. A mean N_2O EF of 0.08 ± 0.01 g kg^{-1} is also reported for one flight over Uganda; issues with temperature control of the instrument optical bench prevented N_2O EFs from being obtained for other flights over Uganda. This study has provided new datasets of African biomass burning EFs and MCEs for two distinct study regions, in which both have been studied little by aircraft measurement previously. These results highlight the important intracontinental variability of biomass burning trace gas emissions, and can be used to better constrain future biomass burning emission budgets. More generally, these results highlight the importance of regional and fuel-type variability when attempting to spatially scale biomass burning emissions. Further work to constrain EFs at more local scales and for more specific (and quantifiable) fuel types will serve to improve global estimates of biomass burning emissions of climate-relevant gases.

10

360

365

370

375

380

385

390

11

1. Introduction

395

The atmospheric burdens of the greenhouse gases (GHGs) CO_2, CH_4 and N_2O have been increasing since the onset of the Industrial Revolution. It is widely accepted that this increase is driven by anthropogenic emissions arising from rapid industrialisation and socio-economic development (Montzka et al. 2011; Ciais et al. 2013). However, there is significant uncertainty about the budgets of these greenhouse gases, as their sources and sinks, both natural and anthropogenic, remain

400 poorly constrained. In particular, the continued growth in atmospheric methane since a period of stagnation from 1999-2006, alongside the concurrent shift in $^{13}CH_4/^{12}CH_4$ isotopic ratio, has yet to be accounted for (Nisbet et al. 2016, 2019; Turner et al. 2019; Schaefer. 2019). In order to accurately attribute the causes of the growth in greenhouse gas burdens, whether from increased sources or reduced sinks, all emission sources need to be quantified with accuracy and precision, and with fine detail in temporal and spatial variability.

405

Biomass burning is a major source, known to contribute significantly to the global budgets of many atmospheric trace gases and aerosols. In addition to CO_2, incomplete combustion of biomass fuel produces both methane and CO, as well as N_2O. It has been estimated that 1.6–4.1 Pg of CO_2, 11–53 Tg CH_4 and 0.1–0.3 Tg of N_2O are emitted to the atmosphere annually as a result of biomass burning on a global scale (Crutzen and Andreae. 2016). The contribution of biomass burning to global GHG budgets

410 will likely increase over time due to climate warming and more widespread drought-stress conditions which increase the likelihood and spread of wildfire events (Liu et al. 2014).

It is estimated that Africa accounts for approximately 52% of all biomass burning carbon emissions, with the Northern Sub-Saharan African region alone accounting for 20-25% of global biomass burning carbon emissions (van der Werf et al. 2010;

415 Ichoku et al. 2016). Many or most of these fires are anthropogenic in origin and are started deliberately for reasons such as clearing land for agricultural use, crop waste burning, management of natural savannah vegetation, or as pest control (Andreae. 1991). Other fires may simply be accidental (e.g. cigarette disposal). Anthropogenic fires are typically lit in the winter dry season. Natural fires, lit by lightning, can occur in the first early summer wet season thunderstorms over dry growth from the previous year. Despite the importance of the African contribution to global biomass burning emissions, there are limited in

420 situ studies of African wildfire emissions.

The UK Natural Environment Research Council (NERC) Methane Observations and Yearly Assessments (MOYA) project is focused primarily on closing the global methane budget through new in situ observations and analysis of existing datasets. This is being achieved (in part) through targeted field campaigns to constrain poorly-quantified methane sources on local and

425 regional scales, as well as the use of atmospheric chemical transport models, such as GEOS-CHEM, to provide global estimates

12

of methane emission trends (Bey et al. 2001; Holmes et al. 2013; Saunois et al. 2016).

This paper presents the results of airborne surveys conducted over regions of Senegal and Uganda with high prevalence of biomass burning events. Two aircraft-based field campaigns, using the UK Facility for Airborne Atmospheric Measurements Atmospheric Research Aircraft (FAAM ARA), were conducted in widely separated parts of Northern Sub-Saharan Africa as part of the MOYA project. The first was based in Senegal between 27 February 2017 and 3 March 2017, and the second based in Uganda between 16 January 2019 and 30 January 2019 (henceforth referred to as MOYA-I and MOYA-II for the 2017 and 2019 campaigns respectively).

The primary focus of the Senegal campaign was to study fires in the winter dry season. The focus in the Ugandan campaign, which was carried out in the brief January dry season, was on equatorial wetlands, with the aim of quantifying methane emissions from these sources using regional-scale flux techniques (O'Shea et al. 2014; Heimburger et al. 2017), but the study of fires of opportunity in the savannah of Northern Uganda was also a major target. The aircraft campaigns also aimed to provide emission estimates for methane and other trace gas and aerosol species from other sources, including anthropogenic emissions from Kampala.

In particular, Emission Factors (EFs) for CH_4, CO_2, N_2O and CO can be determined from the enhancement in trace gas mixing ratio observed when a biomass burning plume was intercepted. These EFs were calculated for multiple fires observed in Senegal and Uganda. A comparison is made between these Senegalese and Ugandan EFs, to assess and interpret intracontinental variability. Comparisons are also made between EFs determined in this study and EFs from Andreae (2019), who includes up to 50 studies reporting fire EFs and modified combustion efficiencies from multiple biomass burning types, such as tropical forest burning, savannah and grassland burning and agricultural residue burning.

13

2. Description of Flights and Methods

2.1. MOYA-I: Senegal 2017

During the first MOYA flying campaign (MOYA-I), four research flights (flight numbers C004, C005, C006 and C007) were conducted using the UK Facility for Airborne Atmospheric Measurement (FAAM) BAe 146-301 Atmospheric Research Aircraft (ARA) to specifically sample fire plumes from biomass burning. The ARA was based in Dakar for the duration of this flying campaign. Near-field biomass burning plumes were sampled in C004 and C005 above the Casamance region of wooded savannah in the south-west of Senegal, and longer-range biomass burning outflow for a wider West African region were sampled in C006 and C007 over the Atlantic seaboard.

Fig. 1 shows the NASA MODerate Resolution Imaging Spectrometer (MODIS) satellite retrievals of locations that were actively burning during the MOYA-I fire sampling flights, which both took place between 28 February 2017 and 2 March 2017. Several straight-and-level (constant altitude and heading) runs were made in the central Casamance region of south-west Senegal, to sample near-field biomass burning emissions from directly above the source fires. Straight and level runs were also carried out during flights C006 and C007 but aimed to sample longer-range regional outflow of biomass burning emissions from the wider inland area of interest.

Visual observation during low passes (<200m) in the flight showed that the fires were in wooded savannah terrain, in winter-dry and winter-brown forest tracts. The forests have been described by de Wolf. (1998) and by Fredericksen et al. (1992). The likely fuels were C3 forest leaf litter and dropped branches as well as savannah grass. The Casamance forests in the overflown area were typically low trees with a generally open canopy. A photograph of one of the near-field fires sampled during flight C005 is shown in Fig. 2

2.2. MOYA-II: Uganda 2019

The flying campaign in Uganda (MOYA-II) took place in late January 2019, a relatively dry month, when northern Uganda experiences its winter dry season, and equatorial southern Uganda is in a short January dry period. The aircraft was based at Entebbe, located on the equator. Two dedicated biomass burning sampling research flights were conducted (flight numbers C133 conducted on 28 Jan 2019 and C134 conducted on 29 Jan 2019), which targeted burning occurring in the north-west of Uganda. Fig. 1 shows the flight tracks and MODIS-retrieved fire locations for the MOYA-II flights. The fires were concentrated

14

towards the north of Uganda in this period.

Fig. 1 shows both dedicated biomass burning sampling flights (C133 and C134), which focussed on the north-western corner of Uganda. This region is far enough north (around 3°N) to experience dry season northern-hemisphere winter. A box pattern was flown around the region, including several passes downwind of fires in the area seen with the clover-like flight patterns. In addition to these dedicated fires flights, flight C132 (conducted on 28 January 2019) is also included in emission analyses. This flight was over Lake Kyoga, closer to the equator at about 1.5°N. The primary purpose of flight C132 was to survey biogenic methane emissions from Lake Kyoga and the surrounding wetlands. Flight C132 involved straight-and-level runs across Lake Kyoga. No fires were specifically targeted during this flight but plumes were intercepted from fires over the northern area of Lake Kyoga, as seen by the deviations in the C132 flight path shown in Fig. 1. EFs from these fires are included in this study.

From visual observation, flights C133 and C134 likely included fires mainly burning C4 tropical grasses, and on flight C132 the fuel was likely agricultural crop waste, which presumably included C4 maize waste, a major local crop.

2.3. CH_4, CO_2, CO and N_2O Instrumentation

During the MOYA-I and MOYA-II campaigns, the FAAM ARA was equipped with a suite of instrumentation for high-accuracy and precision trace gas measurement. All airborne trace gas measurements are time synchronized to an on-board time server For CH_4 and CO_2 mole fractions, a Los Gatos Research Fast Greenhouse Gas Analyser (FGGA) was used. This instrument uses a Cavity-Enhanced Absorption Spectroscopy technique and two continuous-wave near-IR diode lasers. A more detailed description of this instrument, along with its modification for airborne measurements, is provided by O'Shea et al (2013). The FGGA was calibrated using 3 calibration gas standards, all of which were traceable to the NOAA/ESRL WMO-X2007 scale for CO_2, and the WMO-X2004A scale for CH_4. Two of these gas standards provide high/low-concentration span calibrations that are linearly interpolated over an entire flight in order to account for instrument drift. The remaining gas standard was used as a target to define instrumental measurement uncertainty across multiple flights. During MOYA-I the FGGA had a data acquisition rate of 1 Hz, whereas in MOYA-II we used an upgraded system with a 10 Hz acquisition rate. Accounting for all sources of uncertainty associated with these instruments, the mean biases and associated 1σ overall uncertainties are estimated to be 0.004 ± 0.431 ppm and 0.04 ± 2.27 ppb for 1Hz CO_2 and CH_4 measurements respectively during MOYA-I, and -0.048 ± 0.626 ppm and -1.22 ± 2.93 ppb respectively for 10 Hz CO_2 and CH_4 measurements during MOYA-II, which have been averaged to 1 Hz prior to analysis.

15

N$_2$O dry-air mole fractions were measured using an Aerodyne Quantum Cascade Laser Absorption Spectrum (QCLAS) as described by Pitt et al. (2016). This instrument uses a single thermoelectrically cooled quantum cascade laser tuned to a wavelength of ~4.5 µm. The QCLAS is calibrated using three calibration gas standards, all of which are traceable to the World Meteorological Organisation (WMO) X2006 calibration scale for N$_2$O. A 1σ uncertainty of 0.58 ppb was estimated for 1 Hz N$_2$O mole fraction measurements during the MOYA-II flights. We only report data for the MOYA-II (Uganda) campaign in this study as this instrument was not fitted to the aircraft during the MOYA-I (Senegal) campaign.

The Aerodyne QCLAS N$_2$O measurements can be impacted by changes in both cabin pressure and aircraft motion. Changes in altitude and hence cabin pressure change the refractive index in the open path section of the laser beam. This leads to normally static optical fringes moving across the spectral baseline of the instrument, introducing both long-term drift and short-term artefacts into the N$_2$O mole fraction data. Sharp changes in aircraft roll angle in tight turns also introduce short-term artefacts as forces acting on optical components cause slight changes in alignment. These issues are described in further detail in Pitt et al. (2016). A further issue encountered solely during the MOYA-II campaign was occasional loss of optical bench temperature control due to the high temperatures experienced within the aircraft during some flights.

Despite these issues, the N$_2$O plumes from which EF could be calculated were sampled at constant altitude with wings-level at constant optical bench temperature. So the instrument issues detailed likely have a minimal influence on data quality during these periods.

Measurements of CO dry-air mole fractions were sampled using an AeroLaser AL5002 Vacuum-UV fast fluorescence instrument. Specifics about the principles of operation for this instrument are provided by Gerbig et al., 1999. The instrument was calibrated in-flight using a gas standard traceable to the NOAA/ESRL WMO-X2014A scale for CO. We have demonstrated that the linear interpolation of in-flight calibrations yields a mean bias <1 ppb with a 2 sigma precision of 1.8 ppb at 150 ppb for 1 Hz CO measurements, when the instrument is operated optimally. However we recently discovered that a faulty inlet drier may have impacted the accuracy of our CO measurements in 2017-19, and yielded a +9 ± 9 ppb bias in our data. The potential impact of this positive bias is further discussed.

Both the Aerolaser CO instrument and the FGGA were mounted within the pressurised cabin of the aircraft within a single 19" rack. Air was sampled by means of a window-mounted rearward facing inlet comprising of 3/8" PFA tubing housed within 1/2" stainless steel tubing for the CO inlet, and 3/8" stainless steel tubing for the FGGA inlet (O'Shea et al., 2013; Gerbig et al., 1999).

2.4. HCN and HNCO Instrumentation (Chemical Ionisation Mass Spectrometer)

560 The University of Manchester Time of Flight Chemical Ionisation Mass Spectrometer (ToF-CIMS) that has been described in detail by Priestley et al. (2018a; 2018b) for ground-based deployment has recently been modified and certified for use on the FAAM ARA and was used for real time detection of hydrogen cyanide (HCN) and isocyanic acid (HNCO) in this study. The instrument and its subsequent modification is described in detail here, as this study presents the first measurements from the modified ToF-CIMS aboard the FAAM ARA. The original instrument was manufactured by Aerodyne Research Inc. and

565 employs the ARI/Tofwerk High Resolution Time of Flight Mass Spectrometer. Briefly, iodide ions cluster with sample gasses creating a stable adduct that is analysed using time of flight mass spectrometry, with an average mass resolution of 4000 (m/Δm).

The inlet design was based on the configuration characterised by Le Breton et al. (2015), an atmospheric pressure, rearward

570 facing, short residence time inlet, consisting of a 3/8" diameter polytetrafluoroethylene (PTFE) tubing with a total length to the instrument of 48 cm and based on the design shown in Lee et al. (2018). A constant flow of 12 SLM is mass flow controlled to the ion-molecule reaction region (IMR) using a rotary vane pump (Picolino VTE-3). 1 SLM is then subsampled into the IMR for measurement. An Iris system as described by Lee et al. (2018) was then employed to pressure and mass flow control the sample flow into the instrument, avoiding sensitivity changes that would be associated with large variations in pressures in

575 flight that is not controlled sufficiently by the constant flow inlet. This works upon the principle of the manipulation of the size of the critical orifice in response to changes in the IMR pressure. As with the Lee et al. (2018) design, this works by having a stainless-steel plate with a critical orifice and a movable PTFE plate on top of this, also with a critical orifice. These orifices either align fully and allow maximum flow into the instrument or misalign to reduce flow. This movement is controlled by the 24VDC output of the IMR Pirani pressure gauge in relation to the set point and the control unit was designed collaboratively

580 with Aerodyne Research Inc. The IMR set point was 80 mbar for the MOYA campaign, which is set through a combination of pumping capacity on the region (Agilent IDP3), mass flow-controlled reagent ion flow and sample flow. The reagent ion flow is 1 SLM of ultra-high purity (UHP) nitrogen mixed with 2 SCCM of a pressured known concentration gas mix of CH_3I in nitrogen, passed through the radioactive source, [210]Po. The total flow through the IMR is measured (MKS MFM) at the exhaust of the Agilent IDP3 pump so that not only the IMR pressure is monitored but the sample flow also. All mass flow controllers

585 and mass flow meters are measured and controlled using EyeOn. The 1σ variability in the IMR pressure during MOYA is 4% and 6% in the sample flow.

A standard Aerodyne pressure controller is also employed on the short segmented quadrupole (SSQ) region, with two purposes, easily setting the required pressure during start up but to also make subtle adjustments in this region should the IMR pressure

590 change significantly. This works upon the principle controlling an electrically actuated solenoid valve in a feedback loop with

the SSQ pressure gauge to actively control a leak of air into the SSQ pumping line. The SSQ is pumped using Ebara PDV 250 pump and held at 1.8 mbar. The 1σ variability in the SSQ pressure during MOYA is <1%.

Instrument backgrounds are programmatically run for 6 seconds every minute for the entire flight, by overflowing the inlet at the point of entry into the IMR with UHP nitrogen. Here a 1/16th PTFE line enters through the movable PTFE top plate, ensuring that the flow exceeds that of the sample flow. Inlet backgrounds are often run multiple times during flights manually by overflowing as close to the end of the inlet as possible with 20 SLM. Data is taken at 4Hz during a flight, which is routinely averaged to 1 Hz for analysis. Of the 6 points in each background, the first 2 and last point are unused and the mean of the background is calculated using custom python scripting. Using linear interpolation, a time series of the instrument background is determined, humidity corrected if required and then subtracted to give the final time series of each measured mass. Instrument sensitivity to increased humidity changes influences the sensitivity of the instrument to HCN and corrections are applied here to correct both the instrumental backgrounds and final time series of HCN reported here. Only qualitative HCN and HNCO data is reported here as quantitative data is not required for the approach of plume identification used in this study.

The CIMS instrument analysis software (ARI Tofware version 3.1.0) was utilized to attain high resolution, 1Hz, time series of the compounds presented here. For the UMan CIMS, mass-to-charge calibration was performed for 5 known masses; I-, I-.H$_2$O, I-.HCOOH, I$_2$-, I$_3$-, covering a mass range of 127 to 381 m/z. The mass-to-charge calibration was fitted to a 3rd order polynomial and was accurate to within 2 ppm. HCN and HNCO in this case were identified with a 1 ppm error.

2.5 Whole Air Sampling and Methane Isotopic Analysis

Whole air sample (WAS) were collected onboard the aircraft in 3L silica passivated stainless steel canisters (Thames Restek, UK). Sample collection was triggered manually to sample within and outside of fire plumes, guided by the real time methane measurements from the FGGA onboard and visual identification of when the plumes were being crossed. Fill times when sampling the fire plumes ranged between 10 and 40 seconds depending on sampling altitude, representative of an integrated air sample over a 1 - 4 km track. WAS sampling start and end times are recorded using the time on the FAAM ARA on-board time server. Methane mole fraction in the WAS flasks was measured in the Royal Holloway greenhouse gas laboratory using a Picarro 1301 cavity ringdown spectroscopy analyser, and methane isotopic analysis (δ^{13}C) was carried out by gas chromatography – isotope ratio mass spectrometry using a Trace Gas preconcentrator and Isoprime mass spectrometer (see Fisher et al., 2006 for details of the technique).

18

2.6 Calculation of Emission Ratios and Emission Factors

625

In order to select when sampled air was influenced by biomass burning emissions, HCN and CO were used as biomass burning tracers. HCN was chosen as it is almost exclusively emitted from biomass burning, representing 70-85% of the total global HCN source (Li et al. 2003) and has a sufficiently long atmospheric lifetime (relative to advection timescales prior to sampling) of 2-4 months, making HCN a suitable inert tracer for characterising biomass burning plumes (Li et al. 2000).

630

Like HCN, significant amounts of CO, which has an atmospheric lifetime of 1-3 months (Ehhalt et al. 2001), are emitted from biomass burning. CO is also emitted by vehicles, primarily petrol-fuelled and less so by diesel. However, it is likely that biomass burning is the dominant source of carbonaceous emissions in rural areas of Africa as studied here, whereas vehicular carbon emissions are likely concentrated towards urban centres (Gatari et al. 2003). HCN was used as a biomass burning tracer
635   for the MOYA-II (Uganda) analysis. However, as the ToF-CIMS was not fitted to the aircraft during the MOYA-I campaign, no HCN measurement is available for this dataset, and hence CO is used as the biomass burning tracer for MOYA-I analysis.

In order to quantify biomass burning emissions from the enhancements in trace gas mole fraction seen in fire plumes, Emission Ratios (ERs) and EFs were calculated for each species in each fire plume. In this case, an ER is defined as the ratio of a species
640   X relative to a reference species Y. The reference species chosen for this work was CO, as it is relatively inert in the timescale of these measurements, had a relatively stable regional background concentration during these campaigns, and in these rural field areas is almost exclusively emitted during combustion processes and not by other sources such as vehicles (Andreae and Merlet. 2001). The expression for ER calculation is shown in Eq. (1).

645

$$ER_{\frac{X}{CO}} = \frac{\Delta X}{\Delta CO} = \frac{X_{plume} - X_{background}}{CO_{plume} - CO_{background}} \qquad (1)$$

ERs calculated using this approach are also referred to as Normalised Excess Mixing Ratios (NEMRs). When fresh plumes are sampled close to source as they are in the near-field sampling flights, NEMRs can be treated as ERs, calculated using Eq.
650   (1). However in aged plumes, this approach cannot be used to calculate ER, and NEMR is no longer equal to ER. This is due both to chemical processes within the plume that can change composition as well as mixing of background air into plume air (Andreae and Merlet. 2001; O'Shea et al. 2013; Yokelson et al. 2013). HYSPLIT back-trajectory analysis of the MOYA-I far-field flights show that the plume age is <12 hours for flight C006, hence chemical ageing of biomass burning emissions is unlikely to significantly impact the ER calculation for this flight. Plume ages during flight C007 are more variable, and can
655   exceed 2 days in some cases, so ageing may have occurred. This is discussed in further detail in Sect. 3.2. All near-field flights sample biomass burning emissions at the source, so no plume ageing is assumed. Eq. (1) can therefore be used to calculate

19

ERs confidently for most flights.

In order to calculate ERs for near-field biomass burning plumes, a baseline mixing ratio ($X_{background}$) was calculated as the average mixing ratio over 10 seconds of sampled data to either side of each detected plume. The same baseline data periods chosen for each plume were used for all gas species, to ensure that ERs were comparable and not influenced by inconsistent baseline criteria. Despite plumes being selected using a statistical method, the start and the end of each plume as well as the background regions were chosen manually. The area under the plume was then determined by integrating the peak in the concentration versus time data series, giving a total plume concentration (X_{plume}). These values were then used in Eq. (1), along with the corresponding values for CO, to determine an ER. Due to the absence of individual sharp enhancements resolved for specific fire plumes in the far-field flights, a least-squares linear regression of all in-plume points of X versus in-plume points of CO is used to determine ERs for the far-field flights. The ER is equal to the slope of this linear regression. The plume integration and linear regression ER calculation methods are compared in the supplementary information.

Using the calculated ER for each species, EFs were calculated using the carbon mass balance technique (Ward et al. 1984; Radke et al. 1988) An EF is defined as the mass of species emitted (in grams) per kilogram of dry matter burnt. The expression for calculating emission factor is given in Eq. (2).

$$EF_X = F_C \cdot 1000(g\ kg^{-1}) \cdot \frac{M_X}{M_C} \frac{C_X}{C_{total}} \tag{2}$$

where F_C is the mass fraction of carbon in the dry fuel. A value of 0.475 was assumed in this work to best represent African biomass carbon content, and a $\pm 10\%$ uncertainty in this value is assumed (Cofer et al. 1996; Ward et al. 1996; Yokelson et al. 2009). M_X is the molecular weight of species X and M_C is the atomic mass of carbon-12. The term $\frac{C_X}{C_{total}}$ is the molar ratio of species X to total carbon in the plume, which is calculated using Eq. (3).

$$\frac{C_X}{C_{total}} = \frac{\frac{ER\ X}{CO}}{1 + \frac{\Delta CO_2}{\Delta CO} + \frac{\Delta CH_4}{\Delta CO}} \tag{3}$$

In Eq. 3, total carbon in the fire plume was assumed to be the sum of CO, CO_2 and CH_4 emitted. However, as all carbon-containing species could not be measured in this study, the total carbon present in the plume may be underestimated by 1-2%

20

(as reported by Yokelson et al. 1999).

690

A statistical threshold approach was used to determine when a biomass burning plume was sampled during flights. For flights where HCN measurements are available, HCN enhancements exceeding seven standard deviations above the local background were used to select data for ER and EF calculation. Where HCN was not available during MOYA-I, a CO threshold of seven standard deviations over the local background concentration was used. For the far-field flights during MOYA-I (C006 and

695   C007) CO mixing ratios exceeding 15 standard deviations above the local background were chosen for analysis.

2.7 Modified Combustion Efficiency

In addition to EF, the modified combustion efficiency (MCE) is another useful parameter that can be calculated for each

700   biomass burning plume. MCE is here defined by Eq. (4).

$$MCE = \frac{\Delta CO_2}{\Delta CO_2 + \Delta CO} \tag{4}$$

705

MCE can be used to determine the degree to which a fire is smouldering or flaming (Ward and Radke, 1993). Higher MCE values (towards 0.99) indicate that burning is purely flaming, whereas lower MCE values in the range 0.65-0.85 indicate that smouldering conditions dominate. The proportion of trace gases (such as CO and CH_4) emitted typically depends on the

710   completeness of combustion, which is to say that more oxidised products are expected from fires with a high degree of flaming. It is therefore useful to investigate the trend between EF and MCE for different fire plumes (Urbanski, 2013). In the following section, we calculate EFs and MCEs for sampled fire plumes in the MOYA-I and MOYA-II campaigns.

715   **2.8 Uncertainties**

The standard error of the mean (SE) and the mean measurement uncertainty (MU) are reported for each mean EF and MCE displayed in Table 1, The SE here is determined from all EF and MCE calculated for a single flight, and represents the variability of EF and MCE within a flight. The MU is propagated from the instrument uncertainties, therefore each EF and

720   MCE from each fire plume sampled has a measurement uncertainty associated with it. The MUs reported in Table 1 are the average of all individual MUs for all fire plumes sampled during a given flight.

21

ER_x is calculated using Eq. (1) by subtracting $CO_{background}$ from CO_{plume}; any CO measurements systematic positive offset would therefore cancel out and not affect the uncertainty of ER_x. The detection of CO_{plume} during MOYA-I is based on the exceedance of either seven or fifteen standard deviations above background; a CO measurements offset on the background may therefore affect this data filtering step; however due the wide dynamic range of CO measurements encountered during the plumes sampling, we believe a bias will have a very minimal effect on the filtered plume data set used in our analysis. Similarly, the calculations of EF_x using Eq. (2) and (3), and MCE using Eq. (4), rely on ΔCO, which is unaffected by CO measurement bias as previously stated.

3 Results & Discussion

In this section, mean EFs and MCEs are reported on a per-flight basis, and the differences in relative EFs and MCE between individual flights and between Senegal and Uganda are discussed.

3.1 Near-Field sampling

3.1.1 MOYA-I

Flights C004 and C005

The near-field Senegalese fire sampling flights (flight C004 and C005) were carried out on 28 February 2017 and 1 March 2017 respectively. The operating area was over the south western Casamance region of Senegal. A time series of trace gas mixing ratios (CO, CH_4 and CO_2) during flight C004 is shown in Fig. 3. An equivalent time series for flight C005 is displayed in the supplementary information in Fig. S1

The $\delta^{13}C$-CH_4 isotopic ratio of biomass burning emissions can provide information on the content of the biomass fuel that is burned. In C4 vegetation (e.g. tropical grassland), $^{13}CO_2$ is concentrated during the photosynthetic pathway, hence C4 plants tend to be enriched in ^{13}C and emissions show a higher $\delta^{13}C$-CH_4 isotopic ratio. C3 vegetation (woody forest) does not involve the same ^{13}C fractionation as C4, therefore emissions show a lower $\delta^{13}C$-CH_4 ratio relative to C3 plants (Brownlow et al. 2017). Chanton et al. (2000) analysed biomass burning emissions via Keeling plot analysis ($\delta^{13}C$-CH_4 vs inverse CH_4 mole fraction) from a range of fuel sources. They found that African grass burning emitted methane with $\delta^{13}C$-CH_4 ranging between -17 ‰ and -26 ‰, whereas African woodland burning produced methane with a $\delta^{13}C$-CH_4 ratio of -30 ‰. For both near-field and far-field MOYA-I flights, whole-air samples were taken of the biomass burning plumes sampled, as well as of the local background. $\delta^{13}C$-CH_4 isotopic ratios and mean CH_4 mole fractions are determined from these whole-air samples. Further detail of this analysis is provided in Sect. 2.5. Keeling plots for all MOYA-I flights analysed in this work are shown in Fig. 4. Flight C005 shows a linear relationship between inverse CH_4 mole fraction (enhanced CH_4) and $\delta^{13}C$-CH_4 signature. This

22

suggests that biomass burning emissions were captured by whole-air sampling during flight C005 One sample taken during flight C004 appears to have an enriched δ^{13}C-CH$_4$ signal, however this is not included in the linear fit as the single point does not conclusively mean a linear relationship is present. The Y-intercept of -33.7 ± 1.1 ‰ agrees well with the Chanton et al. (2000) estimate for African forest burning, and suggests that C3 vegetation (forest) is included in the fuel burned during flight C005 (Dlugokencky et al. 2011, Chanton et al 2000). Unfortunately, flights over mixed sources in Uganda meant that Keeling plot analysis could not be used to determine the isotopic composition of fire emissions in the same way as carried out for Senegal. The Keeling plot for the MOYA-II isotope samples is shown in the supplementary information (Fig. S2)

Table 1 shows the EFs calculated for all species during flight C004 and C005, as well as savannah and grassland and tropical forest fire EFs reported by Andreae. (2019). The methane EFs for C004 and C005 (2.3 ± 0.24 g kg^{-1} and 1.4 ± 0.15 g kg^{-1} respectively) in this region, at the northern fringe of the African moist tropics, is more comparable to the savannah and grassland methane EF (2.7 ± 2.2 g kg^{-1}) averaged from multiple previous studies by Andreae. (2019). Additionally, mean CO EFs (84 ± 8.7 g kg^{-1} for C004 and 61 ± 6.2 g kg^{-1} for C005) are also more comparable to the savannah and grassland CO EF of 69 ± 20 g kg^{-1} than the tropical forest CO EF of 104 ± 39 g kg^{-1} reported by Andreae. (2019).

The magnitude of methane EFs can be affected by multiple factors, such as fuel moisture (affecting combustion efficiency) as well as fuel type (Brownlow et al. 2017). It is worth noting that the majority of studies included in the Andreae (2019) tropical forest analysis focus on burning associated with Amazonian deforestation, which consists mostly of broad-leafed evergreen forest. In contrast, the Casamance region consists of facultatively deciduous broad-leafed forested savannah, which was observed from the aircraft and is shown by the land cover map in Fig. 5a. It is thus possible that any forest matter burned during the MOYA-I flights consists of dry leaf-litter fuel, whereas the Andreae (2019) study comprising mostly Amazonian land clearing may have included burning of whole evergreen tree structures. In addition to this, the modified combustion efficiencies of the C004 and C005 fires (0.93 ± 0.0031 and 0.95 ± 0.0030 respectively) are both higher than that reported in Andreae (2019) for tropical forest (0.91 ± 0.03), and are more comparable with the Andreae (2019) MCE for savannah and grassland burning (0.94 ± 0.02). This is likely due to the lower fuel moisture content of dry leaf-litter and savannah grasses as opposed to Amazonian evergreen, hence the methane EFs are likely driven by combustion efficiency.

From the EF and δ^{13}C-CH$_4$ results from flights C004 and C005, it is likely that the biomass fuel is a mixture of both deciduous forest matter and savannah grasses as inferred from the isotope and EF results, as well as visual observations of forested savannah and the presence of shrubland and open forest in the land cover classification (Fig. 5a).

3.1.2 MOYA-II

Flight C132

23

Flight C132 was undertaken on 28 January 2019, as a survey of the Lake Kyoga wetland area. Two crop waste biomass burning
790   plumes were sampled from two distinct fires in the area (see Fig. 1). A time series of various trace gas mixing ratios during
this flight is shown in Fig. 6.

As seen in Fig. 5, enhancements (relative to background) in all trace gases were observed in the two biomass burning plumes.
However, N_2O mixing ratio data during the two enhancements were discarded due to aircraft turbulence, which may have
795   corrupted data quality. As a result of the discarded data, as well as instrument drift owing to malfunction of the laser coolant
system, N_2O EFs are not reported for flight C132.

Fig. 6b shows the land cover of Uganda where the fire sampling flights were carried out. In agreement with on-board
observations from the aircraft, much of the land surrounding Lake Kyoga is classified as cropland, and the fuel for the fires
800   appeared to be primarily crop waste. This is a major farming region, with the main crops including maize (a C4 plant) and
cassava (C3) south of Lake Kyoga, and sorghum (C4) north of the Lake. (FEWS NET. 2019). The mean EFs calculated for
C132 (5.2 ± 0.55 g kg^{-1} for CH_4, 1554 ± 164.2 g kg^{-1} for CO_2 and 109 ± 11.3 g kg^{-1} for CO) agree within overlapping uncertainty
with mean agricultural burning EFs of 5.7 ± 6.0 g kg^{-1} for CH_4, 1430 ± 240 g kg^{-1} for CO_2, and 76 ± 55 g kg^{-1} for CO reported
by Andreae (2019). The mean MCE obtained for the C132 fires (0.90 ± 0.0042) is also in agreement with the Andreae (2019)
805   MCE for agricultural residue burning (0.92 ± 0.06). Furthermore, compared to Northern Uganda, the Lake Kyoga region has
a shorter dry season, and higher rainfall. In addition, the fires were bordering a wetland area. Thus the moister conditions of
the Lake Kyoga fires could have resulted in lower temperature, moister combustion and therefore more incomplete burning.

Flights C133 and C134
810   Flights C133 and C134 were dedicated fire sampling flights surveying the winter savannah of north-west Uganda. Both flights
involved box-patterns flown over this region, with deviations taken in order to sample biomass burning plumes visibly
identified over the course of the flights. C133 and C134 were undertaken on 28 January 2019 and 29 January 2019 respectively.
The trace gas time series for these flights are shown in the supplementary information in Fig. S3 and Fig. S4.

815   The CH_4, CO_2 and CO EFs determined for the fire plumes encountered during flight C133 (2.8 ± 0.30) g kg^{-1}, 1620 ± 171.2)
g kg^{-1} and 72 ± 7.4 g kg^{-1} respectively) agreed well with Andreae. (2019) savannah burning EFs (2.7 ± 2.2 g kg^{-1} for CH_4, 1660 ± 90 g kg^{-1} for CO_2 and 69 ± 20 g kg^{-1} for CO). The mean CH_4 and CO_2 EFs for C134 (3.1 ± 0.22 and 1609 ± 173.8 g kg^{-1}
respectively) are broadly comparable with the CH_4 and CO_2 EFs calculated for C133. Additionally, the mean MCE for C134
(0.93 ± 0.0042) is comparable to that of C133 (0.94 ± 0.0041). The mean MCE for C133 and C134 demonstrate that the
820   burning observed in these flights was characterised by more complete flaming combustion than that observed in flight C132
(0.90 ± 0.0042), resulting in the comparatively higher CO_2 EFs and lower CH_4 EFs determined for C133 and C134 relative to

24

C132. The trends in mean MCE and EFs observed during C132, C133, and C134 suggest that EFs are mostly determined by the completeness of combustion over other factors, which is illustrated by the linear relationships between CH_4, CO_2 and CO EFs vs MCE shown in Fig. 7. In particular, fires sampled during C134 may have had a larger smouldering component and they appeared to have involved less complete combustion on average than in C133, which would explain the lower emissions of more highly oxidised CO_2 and higher emissions of more reduced CH_4 than were observed in C134.

The ratio of HCN enhancement to HNCO enhancement within the plumes is informative to quantify combustion completeness and in order to provide redundancy in estimating fire combustion efficiency. Molar ratios of HCN to HNCO in fire emissions have been shown to decrease linearly with increasing combustion temperature (Hansson et al., 2004). Hence lower $\Delta HCN/\Delta HNCO$ ratios should be expected from fires with more complete combustion. Fig. 8a shows $\Delta HCN/\Delta HNCO$ decreasing linearly ($R^2 = 0.36$) with increasing modified combustion efficiency for the MOYA-II fires. Consequently, Fig. 8b shows methane emission factor decreasing with lower $\Delta HCN/\Delta HNCO$ ratio. This further affirms that difference in combustion completeness is the primary driver of methane EF variability observed during MOYA-II. Unfortunately, A similar analysis could not be carried out for MOYA-I as the ToF-CIMS was not fitted to the aircraft during the MOYA-I flights.

As in flight C132, N_2O measurements for flight C133 were unreliable and data were discarded due to the effects of aircraft motion on the instrument optical bench during turbulence. Furthermore, issues with the temperature control of the QCLAS optical bench meant that the baseline noise and drift of the N_2O signal increased during this flight. This resulted in a reduced signal-to-noise ratio of N_2O in the plume. For these reasons, an N_2O EF is not reported for flight C133. However, optical bench temperature control was adequate during flight C134, and aircraft turbulence did not impact N_2O data quality significantly during sampling of some fire plumes. Hence calculation of N_2O EFs was possible for six of the nine fire plumes sampled during flight C134.

In general, the N_2O mixing ratio enhancements in the fire plumes are small (<10 ppb) relative to the background variability (and instrumental noise) of the N_2O dataset (up to 2 ppb). Hence the signal-to-noise ratios of the in-plume N_2O enhancements are poorer than the in-plume enhancements of other species. As a result of this, the uncertainty relative to the mean N_2O EF for C134 is larger than those seen in the other species measured. Despite the combination of instrument issues and poor signal-to-noise ratio, the N_2O EF for flight C134 (0.08 ± 0.01 g kg^{-1}) agrees within overlapping uncertainty with the savannah fire N_2O EF reported by Andreae (2019) (0.17 ± 0.09 g kg^{-1})

Fig. 7 shows strong linear relationships between MCE and CH_4, CO_2 and CO EFs for both MOYA-I and MOYA-II. There is no discernible linear relationship between the N_2O EFs from C134 and MCE, which is shown in the supplementary information in Fig. S5. It is worth noting that CH_4 EFs and corresponding MCE for the far-field flights C006 and C007 are not included in

Fig. 7, as the EFs from these flights are representative of multiple fires with a mixture of phases, whereas the near-field EFs are representative of single fires with a single combustion efficiency associated with them. This trend is expected as higher MCE, and hence more complete flaming combustion, would lead to increased emission of more oxidised combustion products (CO_2) and less emission of more reduced compounds such as CH_4. Despite this, CH_4 EFs measured in Uganda appear to be significantly higher than those measured in Senegal at the same MCE, hence methane emissions from the Ugandan wildfires sampled appear to be higher, and this difference is independent of combustion efficiency. The difference in the linear regressions could possibly be accounted for by differences in the Senegalese and Ugandan fuel mixtures. However, due to detailed analysis of the fuel burned in this study being impossible, and with the likelihood of the fuel source being mixed, the effect of differing fuel content is difficult to quantify. An additional hypothesis is that higher average soil moisture in northern Uganda compared to south-west Senegal could result in soil parching and consequent release of methane-rich air from the soil surrounding wildfires, however more work is required to investigate if soil moisture could affect wildfire methane EFs in this way.

3.2 Far-Field sampling

Flights C006 and C007 were designed to characterise the regional continental outflow of air masses influenced by biomass burning from Senegal and wider West Africa. C006 and C007 involved sampling at various altitudes from 16 m above sea level (ASL) to 6500 m ASL over the West African Atlantic coastline. C006 involved straight-and-level runs directly west of the Casamance region of Senegal targeted during the near-field flights C004 and C005. A strong measured easterly wind indicated continental outflow from the southwest Casamance region of Senegal during flight C006. Sampling during flight C007 was conducted further south, running parallel to the coastline of Guinea-Bissau due to the more complex meteorology encountered during the flight.

In order to identify the approximate origin and age of the biomass burning emissions sampled during the far-field flights, the National Oceanic and Atmospheric Administration (NOAA) HYbrid Single-Particle Lagrangian Integrated Trajectory (HYSPLIT) model was used to calculate 3-dimensional single-particle back-trajectories of air masses sampled during C006 and C007 (Stein et al. 2015). HYSPLIT back-trajectories were run at 60 second intervals during times where biomass burning emissions were sampled (Supplementary: Fig. S6 and S7). The back-trajectories for C006 shown in Fig. 9a and 9b indicate that the age of the biomass burning plumes sampled was approximately 8 hours. Furthermore, the sampled air mass appeared to have advected over the south-western Casamance region, with the highest CO concentrations observed in air masses that passed directly over this region. Thus, the sampled outflow represents a well-mixed air mass influenced by the fire regions targeted in the near-field. The HYSPLIT back-trajectories for C007 shown in Fig. 9c and 9d highlight the much more complex atmospheric dynamics influencing the sampled air masses during flight C007 as opposed to C006. The biomass burning emissions sampled during C007 originated from Guinea-Bissau, Guinea, Sierra Leone, and South Western Senegal, all of

26

which were undergoing active burning during this time as shown in Fig 1a. With these complex air masses, the approximate age of the biomass burning emissions observed in C007 was estimated to be older than that in C006, with an approximate age of 1-2 days. Consequently, the emissions sampled in C007 were representative of a wider area of West African biomass burning than C006, spanning from south-west Senegal down to Sierra Leone. Due to the significantly older plume age of the C007 biomass burning emissions, it is possible that significant chemical aging and/or mixing of background air with plume air has occurred, and hence the ERs or EFs derived from this flight may not be representative of single source regions (see Sect. 2.6).

Box-whisker altitude profiles for flight C006 and C007 are shown in Fig. 10. Fig. 10c shows peak CO concentrations in air masses at approximately 1600 m ASL during flight C006. This is consistent also with fire plume injection heights observed during near-field sampling. Both CH_4 and CO_2 altitude profiles in Fig. 10a and 10b also show enhanced concentrations up to approximately 1600 m ASL, with a rapid decrease in mean CO concentration from 2000 m ASL, indicating free tropospheric air above this. This was confirmed by analysis of measured thermodynamic profiles (not shown in this work). The altitude profiles in Fig. 10d-f show that during flight C007, peak CO concentration as well as the highest mean CO concentration was measured at approximately 1400 m ASL. Concurrently, CH_4 and CO_2 mixing ratios were enhanced up to approximately 3400 m ASL. Above this, CO, CH_4 and CO_2 mixing ratios decreased to background free tropospheric concentrations with comparatively small ranges. In comparison to flight C006, in C007 the biomass burning emissions appeared to be more mixed throughout the polluted boundary layer.

A linear weighted regression was fitted to data points for CH_4 and CO_2 versus tracer-CO (Fig. 11) for samples within the biomass burning plume, using a statistical CO threshold to identify the smoke plumes from fires (as described in Sect. 2.6). The gradient of this fit was equivalent to the ERs with respect to CO and included in Table 1. Fig. 11a and 11b show strong linear trends between in-plume CH_4 and CO_2 vs CO for flight C006. with R^2 values of 0.70 and 0.76 respectively.

Although some degree of linearity is identifiable, the observed trends shown in Fig. 11c and 11d are significantly weaker than those seen for flight C006, with R^2 values of 0.14 for CH_4 vs CO and 0.49 for CO_2 vs CO. The higher variance in the C007 linear regressions, when compared with C006, could be attributed to mixed phases of burning and/or mixed degrees of chemical aging present within the same biomass burning influenced air mass. Therefore homogenisation of species from individual fire areas within the whole enhanced plume in C007 may be incomplete, and multiple fire phases with distinct combustion efficiencies or plume aging may explain the poorer fits seen in C007.

As observed in Sect. 3.1 in the near-field sampling flights C004 and C005, the methane EF calculated for C006 (1.6 ± 0.18 g kg^{-1}) and C007 (2.4 ± 0.25 g kg^{-1}) is more comparable to savannah and grassland burning methane EF (2.7 ± 2.2 g kg^{-1} reported

27

by Andreae. (2019)~~), despite the visual observation of burning forest matter and isotopic signature of such.~~ This is attributed to the mixed nature of the fuel source, likely comprising of facultatively deciduous forest litter and savannah grasses

MCE values of 0.94 ± 0.0041 for C006 and 0.96 ± 0.0037 for C007 are also shown in Table 1. It is likely that biomass burning signatures with a higher smouldering component were sampled in C006, which is further evidenced by the lower CO_2 EFs determined for C006. In contrast, the CH_4 EF is higher for C007, in which more complete combustion is inferred from the MCE. It is expected that this is due to the aging of species sampled offshore in a recirculated airmass in C007 (as shown Fig. 12), and hence an indication that ERs and EFs may not be representative of the source fires. Despite ERs and EFs being shown for C007 in Fig. 11c and 11d, the EFs for C007 are not included in the mean calculation for Senegalese biomass burning EFs.

4. Conclusion

Airborne observations of CH_4, CO_2, and CO emissions from biomass burning were carried out in southern Senegal in February/March 2017 and northern Uganda in January 2019. Mean EFs of 1.8 ± 0.19 g kg^{-1} for CH_4, 1633 ± 171.4 g kg^{-1} for CO_2 and 67 ± 7.4 g kg^{-1} for CO were obtained from the Senegalese fires, with a mean modified combustion efficiency of 0.94 ± 0.005. Mean EFs of 3.1 ± 0.35 g kg^{-1} for CH_4, 1610 ± 169.7 g kg^{-1} for CO_2 and 78 ± 8.9 g kg^{-1} for CO were obtained for the Ugandan fires, with a mean modified combustion efficiency of 0.93 ± 0.004. A mean N_2O EF of 0.08 ± 0.01 g kg^{-1} is also reported for six fire plumes sampled over Uganda. CH_4 EFs showed strong linear relationships with modified combustion efficiency for both Senegal and Uganda. The variability in EFs within each study area was attributed to the mixed-phase nature of the fires, with a range of combustion efficiencies observed. These results also suggest that Ugandan fires have a higher methane emission factor for the equivalent combustion efficiency observed for Senegal. This may be a consequence of the difference in fuel between the Ugandan savannah grass and cropland waste fuels, and the Senegalese forest litter and grassland fuel. This highlights the importance of considering both regional and local variability when attempting to spatially scale biomass burning emissions, and suggests that singular regional EF values may lead to inaccurate estimates. Further work to constrain EFs at more local scales and for more specific (and quantifiable) fuel types will serve to improve global estimates of biomass burning emissions of climate-relevant gases.

This work demonstrates the value of airborne measurements for characterising biomass burning emissions from multiple fires over wide areas. This study has provided unique *in situ* datasets in two geographical regions where there has hitherto been little study by aircraft measurement. The results will improve understanding of the role of African biomass burning in the global carbon budget, and the work demonstrates the importance of good knowledge of fuel mixture for the accurate reporting of EFs. This study demonstrates the utility of airborne measurements for characterising biomass burning emissions from multiple fires over wide areas. Further work is required to investigate the link that fire fuel content may have on the emission of methane from biomass burning.

28

Author Contribution

Patrick Barker: Lead author, Data curation, formal analysis, methodology, investigation, validation, writing – original draft, writing - review and editing. Grant Allen: Principal Investigator, project administration, conceptualisation, supervision, funding acquisition, validation, writing – original draft, writing – review and editing. Martin Gallagher: Validation, supervision, writing – review and editing. Joseph R. Pitt: Data curation, formal analysis, validation, supervision. Rebecca E. Fisher: Data curation, formal analysis, investigation, writing – review and editing. Thomas Bannan: Data curation, formal analysis, writing – review and editing. Euan G. Nisbet: Principal investigator, project administration, conceptualisation, funding acquisition, validation, writing – review and editing. Stephane J. -B. Bauguitte: Data curation, formal analysis, validation, writing – review and editing. Dominika Pasternak: Data curation, formal analysis, validation, writing – review and editing. Samuel Cliff: Data curation, formal analysis, validation. Marina B. Schimpf: Data curation, formal analysis, validation. Archit Mehra: Data curation, formal analysis, writing – review and editing. Keith N. Bower: project administration, conceptualisation. James D. Lee: project administration, conceptualisation, writing – review and editing. Hugh Coe: conceptualisation, validation. Carl J. Percival: Data curation, validation, writing – review and editing.

Competing interests

The authors declare no conflict of interest.

References

Andreae, M. O.: Biomass burning: Its history, use and distribution and its impact on environmental quality and global climate, Glob. Biomass Burn. Atmos. Clim. Biosph. Implic., (January 1991), 3–21, 1991.

Andreae, M.: Emission of trace gases and aerosols from biomass burning -- An updated assessment, Atmos. Chem. Phys. Discuss., 2019, 1–27, doi:10.5194/acp-2019-303, 2019.

Ballentine, D., Macko, S. and Turekian, V.: Variability of stable carbon isotopic compositions in individual fatty acids from combustion of C4 and C3 plants: implications for biomass burning, Chem. Geol., 152(1–2), 151–161, 1998.

Bey, I., Jacob, D. J., Yantosca, R. M., Logan, J. A., Field, B. D., Fiore, A. M., Li, Q., Liu, H. Y., Mickley, L. J. and Schultz, M. G.: Global modeling of tropospheric chemistry with assimilated meteorology: Model description and evaluation, J. Geophys. Res. Atmos., 106(D19), 23073–23095, doi:10.1029/2001JD000807, 2001.

Brownlow, R., Lowry, D., Fisher, R. E., France, J. L., Lanoisellé, M., White, B., Wooster, M. J., Zhang, T. and Nisbet, E. G.: Isotopic Ratios of Tropical Methane Emissions by Atmospheric Measurement, Global Biogeochem. Cycles, doi:10.1002/2017GB005689, 2017.

Buchhorn, M., Smets, B., Bertels, L., Lesiv, M., Tsendbazar, N.-E. and Li, L.: Copernicus Global Land Service: Land Cover 100m, epoch 2018, Africa Demo (Version V2.1.1), doi:10.5281/zenodo.3518087, 2019.

Chanton, J. P., Rutkowski, C. M., Schwartz, C. C., Ward, D. E. and Boring, L.: Factors influencing the stable carbon isotopic signature of methane from combustion and biomass burning, J. Geophys. Res. Atmos., doi:10.1029/1999JD900909, 2000.

Ciais, P., Sabine, C., Bala, G., Bopp, L., Brovkin, V., Canadell, J., Chhabra, A., DeFries, R., Galloway, J., Heimann, M., Jones, C., Quéré, C. Le, Myneni, R. B., Piao, S. and Thornton, P.: The physical science basis. Contribution of working group I to the fifth assessment report of the intergovernmental panel on climate change, Chang. IPCC Clim., 465–570, doi:10.1017/CBO9781107415324.015, 2013.

Cofer, W., Levine, J., Winstead, E., Cahoon, D., Sebacher, D., Pinto, J. and Stocks, B.: Source compositions of trace gases released during African savanna fires, J. Geophys. Res. Atmos., 101(D19), 23597–23602, 1996.

Crutzen, P. J. and Andreae, M. O.: Biomass Burning in the Tropics: Impact on Atmospheric Chemistry and Biogeochemical

1020   Cycles, in Paul J.Crutzen: A Pioneer on Atmospheric Chemistry and Climate Change in the Anthropocene, edited by P. J. Crutzen and H. G. Brauch, pp. 165–188, Springer International Publishing, Cham., 2016.

De Wolf, J.: Species composition and structure of the woody vegetation of the Middle Casamance region (Senegal), For. Ecol. Manag., *111*(2-3), pp.249-264, 1998.

Dlugokencky, E. J., Nisbet, E. G., Fisher, R. and Lowry, D.: Global atmospheric methane: Budget, changes and dangers,
1025   Philos. Trans. R. Soc. A Math. Phys. Eng. Sci., doi:10.1098/rsta.2010.0341, 2011.

Ehhalt, D. and Prather, M.: Atmospheric Chemistry and Greenhouse Gases, Clim. Chang. 2001 Sci. Basis, 239–287, doi:10.2753/JES1097-203X330403, 2001.

Facility for Airborne Atmospheric Measurements; Natural Environment Research Council; Met Office (2017): MOYA: ground station and in-situ airborne observations by the FAAM BAE-146 aircraft. Centre for Environmental Data
1030   Analysis, Accessed Mar 2019. http://catalogue.ceda.ac.uk/uuid/d309a5ab60b04b6c82eca6d006350ae6

FEWS NET: Uganda, https://fews.net/east-africa/uganda, Accessed 25 March 2020.

Fisher, R., Lowry, D., Wilkin, O., Sriskantharajah, S. and Nisbet, E. G.: High-precision, automated stable isotope analysis of atmospheric methane and carbon dioxide using continuous-flow isotope-ratio mass spectrometry, Rapid Commun. Mass Spectrom., doi:10.1002/rcm.2300, 2006.

1035   Frederiksen, P. and Lawesson, J.E.: Vegetation types and patterns in Senegal based on multivariate analysis of field and NOAA-AVHRR satellite data, J. Veg. Sci., 3(4), pp.535-544, 1992.

Gatari, M. J. and Boman, J.: Black carbon and total carbon measurements at urban and rural sites in Kenya, East Africa, Atmos. Environ., doi:10.1016/S1352-2310(02)01001-4, 2003.

Hansson, K. M., Samuelsson, J., Tullin, C. and Åmand, L. E.: Formation of HNCO, HCN, and NH3 from the pyrolysis of
1040   bark and nitrogen-containing model compounds, Combust. Flame, doi:10.1016/j.combustflame.2004.01.005, 2004.

Heimburger, A. M. F., Harvey, R. M., Shepson, P. B., Stirm, B. H., Gore, C., Turnbull, J., Cambaliza, M. O. L., Salmon, O. E., Kerlo, A. E. M., Lavoie, T. N., Davis, K. J., Lauvaux, T., Karion, A., Sweeney, C., Brewer, W. A., Hardesty, R. M. and Gurney, K. R.: Assessing the optimized precision of the aircraft mass balance method for measurement of urban greenhouse gas emission rates through averaging, Elementa, 5, doi:10.1525/elementa.134, 2017.

1045   Holmes, C. D., Prather, M. J., Søvde, O. A. and Myhre, G.: Future methane, hydroxyl, and their uncertainties: Key climate and emission parameters for future predictions, Atmos. Chem. Phys., doi:10.5194/acp-13-285-2013, 2013.

Ichoku, C., Ellison, L. T., Willmot, K. E., Matsui, T., Dezfuli, A. K., Gatebe, C. K., Wang, J., Wilcox, E. M., Lee, J., Adegoke, J. and others: Biomass burning, land-cover change, and the hydrological cycle in Northern sub-Saharan Africa, Environ. Res. Lett., 11(9), 95005, 2016.

1050   Le Breton, M., Bacak, A., Muller, J. B., Bannan, T. J., Kennedy, O., Ouyang, B., ... & Daniels, M. J.: The first airborne comparison of N_2O_5 measurements over the UK using a CIMS and BBCEAS during the RONOCO campaign. Analytical Methods, 6(24), 9731-9743, 2014.

31

Lee, B. H., Lopez-Hilfiker, F. D., Veres, P. R., McDuffie, E. E., Fibiger, D. L., Sparks, T. L., ... & Iyer, S.: Flight deployment of a high-resolution time-of-flight chemical ionization mass spectrometer: Observations of reactive

1055   halogen and nitrogen oxide species. J. Geophys. Res: Atmos, 123(14), 7670-7686, 2018.

Li, Q., Jacob, D. J., Bey, I., Yantosca, R. M., Zhao, Y., Kondo, Y. and Notholt, J.: Atmospheric hydrogen cyanide (HCN): Biomass burning source, ocean sink?, Geophys. Res. Lett., 27(3), 357–360, 2000.

Li, Q., Jacob, D. J., Yantosca, R. M., Heald, C. L., Singh, H. B., Koike, M., Zhao, Y., Sachse, G. W. and Streets, D. G.: A global three-dimensional model analysis of the atmospheric budgets of HCN and CH3CN: Constraints from aircraft

1060   and ground measurements, J. Geophys. Res. D Atmos., 108(21), doi:10.1029/2002jd003075, 2003.

Montzka, S. A., Dlugokencky, E. J. and Butler, J. H.: Non-CO 2 greenhouse gases and climate change, Nature, 476(7358), 43–50, doi:10.1038/nature10322, 2011.

Nisbet, E., Dlugokencky, E., Manning, M., Lowry, D., Fisher, R., France, J., Michel, S., Miller, J., White, J., Vaughn, B. and others: Rising atmospheric methane: 2007--2014 growth and isotopic shift, Global Biogeochem. Cycles, 30(9), 1356–

1065   1370, 2016.

Nisbet, E. G., Manning, M., Dlugokencky, E., Fisher, R., Lowry, D., Michel, S., ... & Brownlow, R. Very strong atmospheric methane growth in the 4 years 2014–2017: Implications for the Paris Agreement. Global Biogeochem. Cycles, *33*, 318-342, 2019.

O'Shea, S., Allen, G., Gallagher, M., Bauguitte, S., Illingworth, S., Le Breton, M., Muller, J., Percival, C., Archibald, A.,

1070   Oram, D. and others: Airborne observations of trace gases over boreal Canada during BORTAS: campaign climatology, air mass analysis and enhancement ratios, Atmos. Chem. Phys., 13(24), 12451–12467, 2013.

O'Shea, S., Bauguitte, S., Gallagher, M., Lowry, D. and Percival, C.: Development of a cavity-enhanced absorption spectrometer for airborne measurements of CH 4 and CO 2, Atmos. Meas. Tech., 6(5), 1095–1109, 2013.

O'Shea, S. J., Allen, G., Fleming, Z. L., Bauguitte, S. J.-B., Percival, C. J., Gallagher, M. W., Lee, J., Helfter, C. and Nemitz,

1075   E.: Area fluxes of carbon dioxide, methane, and carbon monoxide derived from airborne measurements around Greater London: A case study during summer 2012, J. Geophys. Res. Atmos., 119(8), 4940–4952, doi:10.1002/2013JD021269, 2014.

Priestley, M., Le Breton, M., Bannan, T. J., Worrall, S. D., Bacak, A., Smedley, A. R., ... & Shallcross, D. E.: Observations of organic and inorganic chlorinated compounds and their contribution to chlorine radical concentrations in an urban

1080   environment in northern Europe during the wintertime. Atmos Chemistry and Physics, 18(18), 13481-13493, 2018.

Radke, L. F., Hegg, D. A., Lyons, J. H., Brock, C. A., Hobbs, P. V, Weiss, R. and Rasmussen, R.: Airborne measurements on smokes from biomass burning, Aerosols Clim., 411–422, 1988.

Saunois, M., Bousquet, P., Poulter, B., Peregon, A., Ciais, P., Canadell, J. G., Dlugokencky, E. J., Etiope, G. and Bastviken, D.: The global methane budget 2000 – 2012, , 697–751, doi:10.5194/essd-8-697-2016, 2016.

1085   Schaefer, H.: On the Causes and Consequences of Recent Trends in Atmospheric Methane, Curr. Clim. Chang. Reports,

doi:10.1007/s40641-019-00140-z, 2019.

Stein, A. F., Draxler, R. R., Rolph, G. D., Stunder, B. J. B., Cohen, M. D. and Ngan, F.: Noaa's hysplit atmospheric transport and dispersion modeling system, Bull. Am. Meteorol. Soc., doi:10.1175/BAMS-D-14-00110.1, 2015.

Turner, A. J., Frankenberg, C. and Kort, E. A.: Interpreting contemporary trends in atmospheric methane, Proc. Natl. Acad. Sci. U. S. A., doi:10.1073/pnas.1814297116, 2019.

Van Der Werf, G. R., Randerson, J. T., Giglio, L., Collatz, G. J., Mu, M., Kasibhatla, P. S., Morton, D. C., Defries, R. S., Jin, Y. and Van Leeuwen, T. T.: Global fire emissions and the contribution of deforestation, savanna, forest, agricultural, and peat fires (1997-2009), Atmos. Chem. Phys., 10(23), 11707–11735, doi:10.5194/acp-10-11707-2010, 2010.

Ward, D. E. and Hardy, C. C.: Advances in the characterization and contril of emissions from prescribed fires, in Proceedings, Annual Meeting - Air Pollution Control Association., 1984.

Ward, D. E. and Radke, L. F.: Emissions Measurements from Vegetation Fires : A Comparative Evaluation of Methods and Results, Fire Environ. Ecol. Atmos. Clim. Importance Veg. Fires, 1993.

Ward, D. E., Hao, W. M., Susott, R. A., Babbitt, R. E., Shea, R. W., Kauffman, J. B. and Justice, C. O.: Effect of fuel composition on combustion efficiency and emission factors for African savanna ecosystems, J. Geophys. Res. Atmos., doi:10.1029/95jd02595, 1996.

Wessel, P. and Smith, W. H. F.: A global, self-consistent, hierarchical, high-resolution shoreline database, J. Geophys. Res. Solid Earth, doi:10.1029/96jb00104, 1996.

Yokelson, R., Goode, J., Ward, D., Susott, R., Babbitt, R., Wade, D., Bertschi, I., Griffith, D. and Hao, W.: Emissions of formaldehyde, acetic acid, methanol, and other trace gases from biomass fires in North Carolina measured by airborne Fourier transform infrared spectroscopy, J. Geophys. Res. Atmos., 104(D23), 30109–30125, 1999.

Yokelson, R., Crounse, J., DeCarlo, P., Karl, T., Urbanski, S., Atlas, E., Campos, T., Shinozuka, Y., Kasputin, V., Clarke, A. and others: Emissions from biomass burning in the Yucatan, Atmos. Chem. Phys., 9(15), 5785, 2009.

Yokelson, R. J., Andreae, M. O. and Akagi, S. K.: Pitfalls with the use of enhancement ratios or normalized excess mixing ratios measured in plumes to characterize pollution sources and aging, Atmos. Meas. Tech., doi:10.5194/amt-6-2155-2013, 2013.

York, D., Evensen, N. M., Martínez, M. L. and De Basabe Delgado, J.: Unified equations for the slope, intercept, and standard errors of the best straight line, Am. J. Phys., doi:10.1119/1.1632486, 2004.

1120

Table 1: Mean CH₄, CO₂, N₂O and CO EFs and MCE for all MOYA-I (Senegal) and MOYA-II (Uganda) fires sampling flights. Both the standard error on the mean and the mean measurement uncertainty (MU) for EFs and MCEs during each flight for each species is also given. EFs and MCEs compiled from studies of tropical forest and savannah biomass burning by Andreae. (2019) are also shown. All EFs are reported in units of g kg⁻¹. *Note that N₂O EFs could only be calculated for six of the nine fire plumes sampled during flight C134.

1125

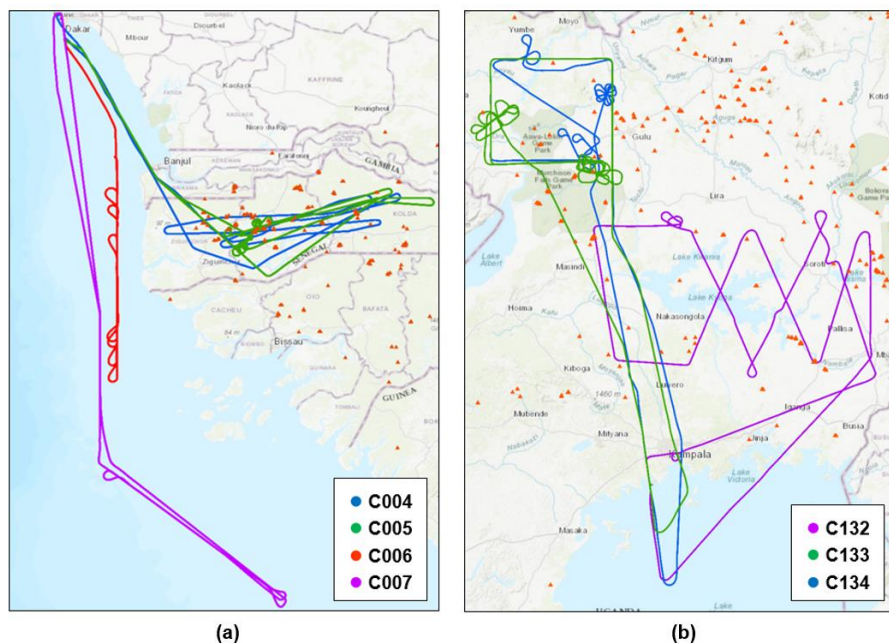|	Flight No	N	CH₄ mean	SE	MU	CO₂ mean	SE	MU	CO mean	SE	MU	N₂O mean	SE	MU	MCE mean	SE	MU
MOYA-I	C004	7	2.3	0.13	0.24	1612	3.4	170	84	2.3	8.7	-	-	-	0.93	0.0047	0.0031
	C005	12	1.4	0.11	0.15	1647	4.3	174	61	2.9	6.2	-	-	-	0.95	0.0024	0.0030
	C006		1.6	-	0.18	1625	-	170	-	-	-	-	-	-	0.94		0.0041
	C007		2.4	-	0.25	1663	-	173	-	-	-	-	-	-	0.96	-	0.0037
MOYA-II	C132	2	5.2	0.15	0.55	1554	4.0	164	109	2.3	11.3	-	-	-	0.90	0.0021	0.0042
	C133	11	2.8	0.21	0.30	1620	7.0	171	72	2.6	7.4	-	-	-	0.94	0.0038	0.0041
	C134	9	3.1	0.70	0.22	1609	23.9	174	79	14.0	8.1	0.08*	0.01	0.01	0.93	0.0128	0.0042
Andreae (2019)	Tropical Forest		6.5	-	1.6	1620	-	70	104	-	39	-	-	-	0.91	-	0.03
	Savannah and Grassland		2.7	-	2.2	1660	-	90	69	-	20	0.17	-	0.09	0.94	-	0.02

1130

34

(a) (b)

Figure 1: FAAM ARA flight tracks of (a) MOYA-I biomass burning sampling flights C004 (Blue), C005 (Green), C006 (Red) and C007 (Purple) over the south western region of Senegal and the Atlantic seaboard. and (b) MOYA-II biomass burning sampling flights C132 (Purple), C133 (Green) and C134 (Blue) over northern Uganda. MODIS infrared satellite retrievals of fires present between (a) 28 February 2017 and 02 March 2017 and (b) 28 January 2019 and 29 January 2019 are also shown (orange triangles). © OpenStreetMap contributors and the GIS User Community 2020. Distributed under a Creative Commons BY-SA License.

35

Figure 2: Photograph of Senegalese wildfire taken from aboard the FAAM ARA during flight C005 of the MOYA-I campaign.

Figure 3: time series of CO (red), CH₄ (black), CO₂ (blue) and concentrations in the plumes analysed for flight C005. Median WAS canister fill times are marked on the CH₄ time series as pink triangles. Note that some WAS taken in background regions are not shown here.
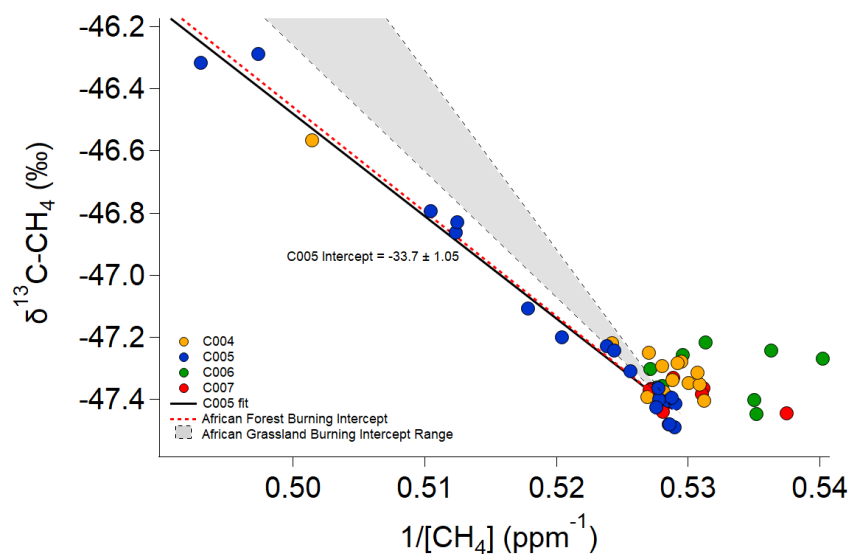
Figure 4: Keeling plot (δ^{13}C-CH$_4$ vs inverse CH$_4$ mixing ratio) for all flights in the MOYA-I (Senegal) analyses. A linear fit of points from flight C005 (blue) is also displayed. Simulated fits of African forest (red dashed line) and grassland (grey shaded area) burning using the intercepts and intercept ranges reported by Chanton et al. (2001) are also shown.
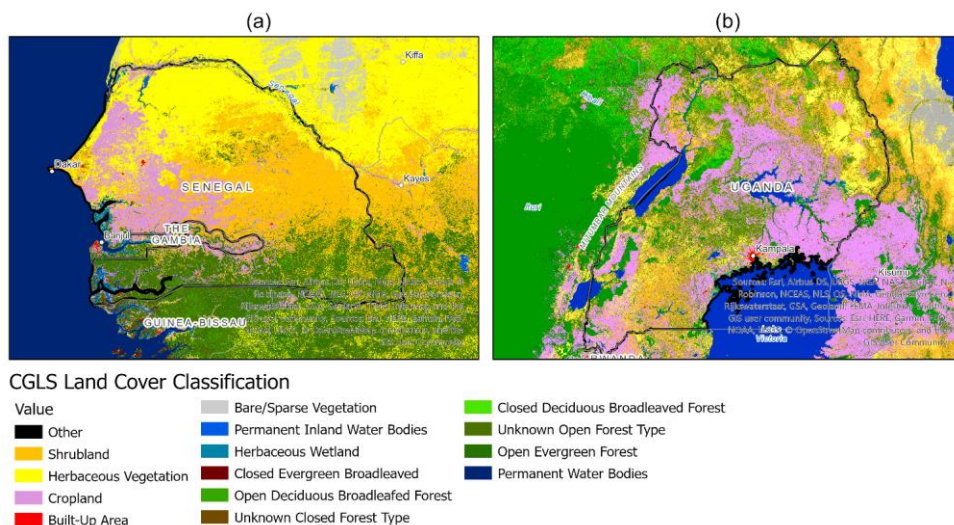
CGLS Land Cover Classification

Value		
■ Other	■ Bare/Sparse Vegetation	■ Closed Deciduous Broadleaved Forest
■ Shrubland	■ Permanent Inland Water Bodies	■ Unknown Open Forest Type
■ Herbaceous Vegetation	■ Herbaceous Wetland	■ Open Evergreen Forest
■ Cropland	■ Closed Evergreen Broadleaved	■ Permanent Water Bodies
■ Built-Up Area	■ Open Deciduous Broadleafed Forest	
	■ Unknown Closed Forest Type	

Figure 5: (a) Land cover classification map of Uganda from 2019. (b) Land cover classification map of Senegal from 2017. Data is obtained from the Copernicus Global Land Service Africa Land Cover Maps, which are derived from PROBA-V satellite observations (Buchhorn et al. 2019). © OpenStreetMap contributors and the GIS User Community 2020. Distributed under a Creative Commons BY-SA License.
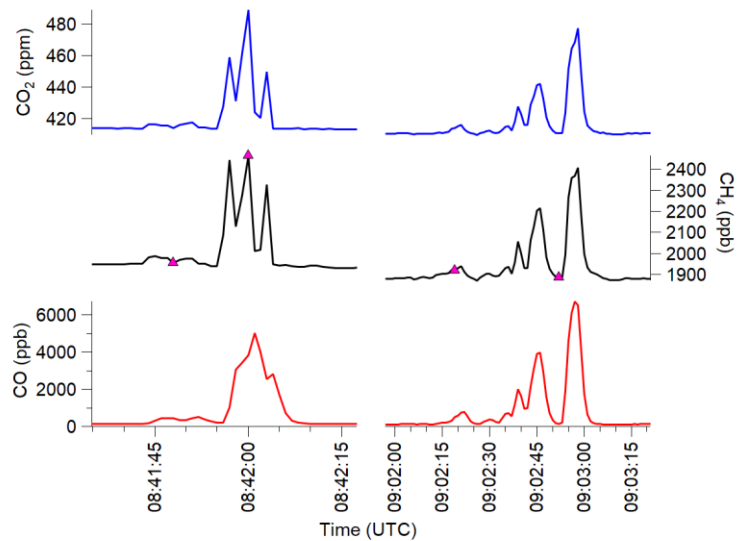
39

Figure 6: time series of CO (red), CH₄ (black), CO₂ (blue) and concentrations in the plumes analysed for flight C005. Median WAS canister fill times are marked on the CH₄ time series as pink triangles. Note that some WAS taken in background regions are not shown here.
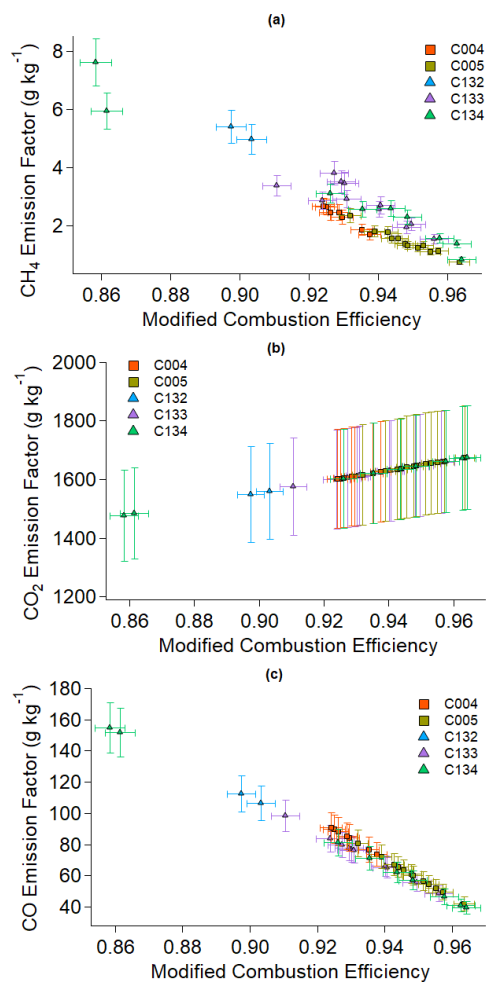
Figure 7: (a) Methane, (b) CO₂ and (c) CO EF vs modified combustion efficiency for all biomass burning plumes sampled over all flights (squares are MOYA-I and triangles are MOYA-II). Points are coloured by flight number.
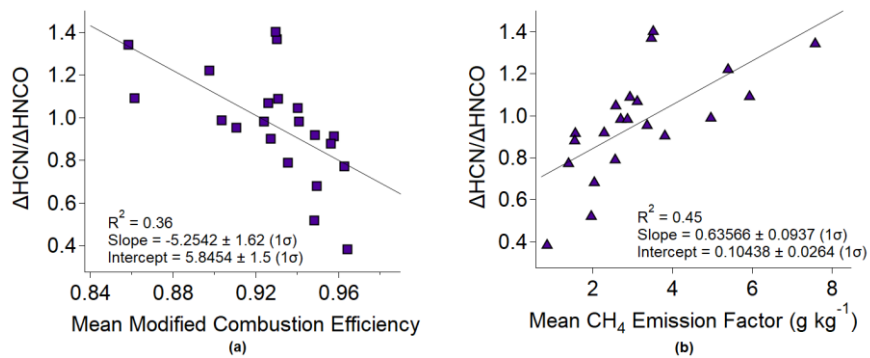
Figure 8: Plot of HCN enhancement over HNCO enhancement in biomass burning plumes vs (a) mean modified combustion efficiency and (b) mean methane EF in g kg^{-1} for all MOYA-II data.
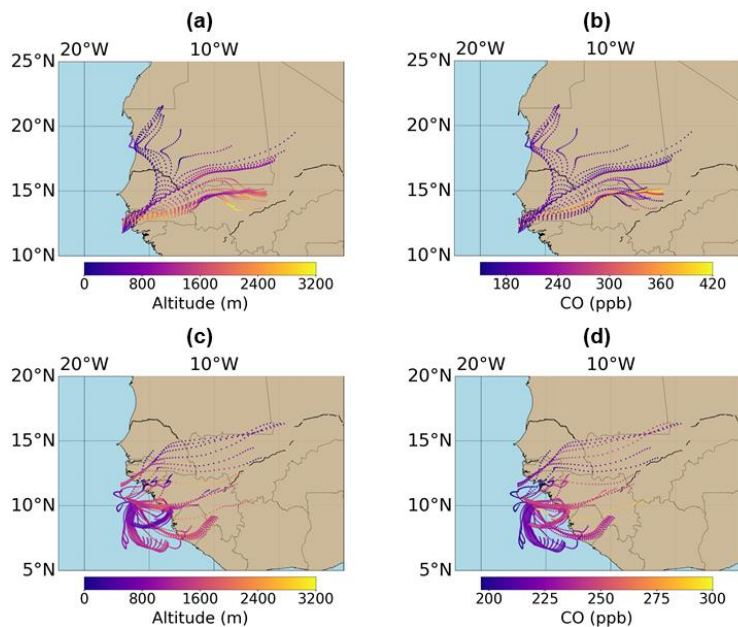
Figure 9: 2-day HYSPLIT back-trajectories from sections of the flight tracks of flight C006 and C007 during which biomass burning emissions were sampled (the in-fire plume data from Fig. 10). The back-trajectories are coloured by (a) trajectory altitude and (b) CO mixing ratio at the trajectory end-point on the flight C006 flight track. (c) and (d) show the back-trajectories for flight C007, coloured by trajectory altitude and CO mixing ratio respectively. Trajectories are run at 60 second intervals of in-plume flight data. The basemaps are obtained from Global Self-consistent, Hierarchical, High-resolution Geography Database (GSHHG) data (Wessel and Smith. 1996).
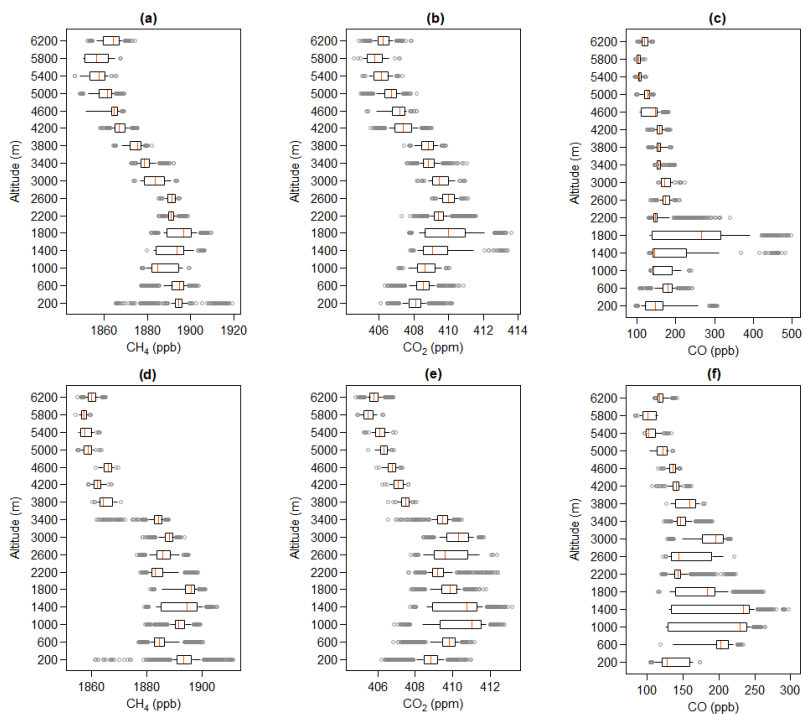
Figure 10. Box-whisker plots of (a) CH$_4$, (b) CO$_2$ and (c) CO altitude profiles for flight C006 and (d) CH$_4$, (e) CO$_2$ and (f) CO altitude profiles for flight C007. Altitude is divided into 400 m vertical bins for all box-whisker plots. The boxes represent the 25th and 75th percentiles, whiskers represent 10th and 90th percentiles, and the grey circular points are outliers.

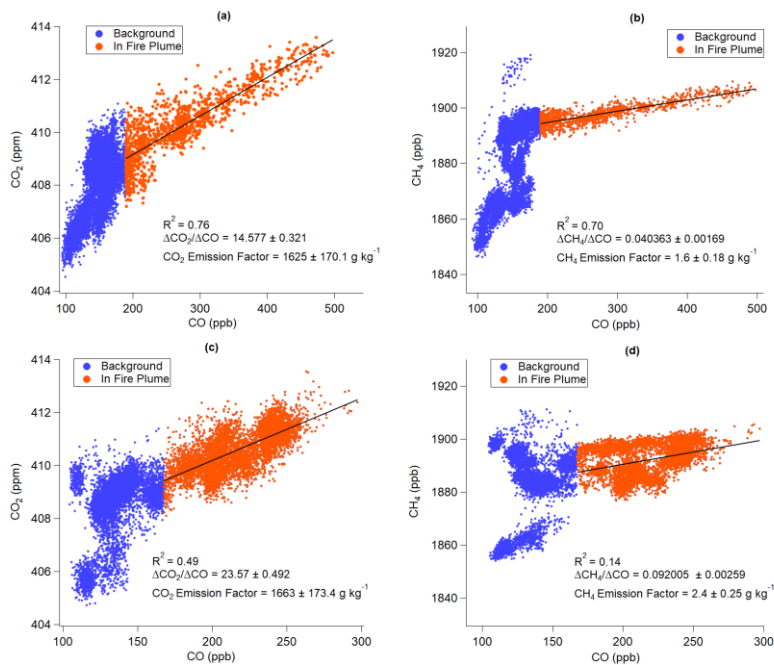**Figure 11: Linear regressions of in-plume (a) CH₄ and (b) CO₂ mixing ratio versus in-plume CO mixing ratio for flight C006 and (c) CH₄ and (d) CO₂ mixing ratio versus in-plume CO for flight C007. The linear regressions are calculated using the York regression method, and are weighted towards CO and CH₄/CO₂ measurement uncertainty (York et al. 2004). ERs obtained from the slope are also shown, as well as the calculated EFs.**